

Interpretation and implication of the non-detection of GeV spectrum excess by Fermi γ -ray Space Telescope in most GRBs

Yi-Zhong Fan^{1,2} *

¹Niels Bohr International Academy, Niels Bohr Institute, University of Copenhagen, Blegdamsvej 17, DK-2100 Copenhagen, Denmark

²Purple Mountain Observatory, Chinese Academy of Sciences, Nanjing 210008, China

27 October 2018

ABSTRACT

Since the launch of the Fermi Gamma-ray Space Telescope on 11 June 2008, significant detections of high energy emission have been reported only in six Gamma-ray Bursts (GRBs) until now. In this work we show that the lack of detection of a GeV spectrum excess in almost all GRBs, though somewhat surprisingly, can be well understood within the standard internal shock model and several alternatives like the photosphere-internal shock (gradual magnetic dissipation) model and the magnetized internal shock model. The delay of the arrival of the > 100 MeV photons from some Fermi bursts can be interpreted too. We then show that with the polarimetry of prompt emission these models may be distinguishable. In the magnetized internal shock model, high linear polarization level should be typical. In the standard internal shock model, high linear polarization level is still possible but much less frequent. In the photosphere-internal shock model, the linear polarization degree is expected to be roughly anti-correlated with the weight of the photosphere/thermal component, which may be a unique signature of this kind of model. We also briefly discuss the implication of the current Fermi GRB data on the detection prospect of the prompt PeV neutrinos. The influences of the intrinsic proton spectrum and the enhancement of the neutrino number at some specific energies, due to the cooling of pions (muons), are outlined.

Key words: gamma rays: bursts – polarization – radiation mechanism: nonthermal – acceleration of particles – elementary particles: neutrino

1 INTRODUCTION

Gamma-ray Bursts (GRBs) are the most extreme explosion discovered so far in the universe. With the discovery of the afterglows and then the measurement of the redshifts in 1997 (see van Paradijs et al. 2000, for a review), the cosmological origin of GRBs has been firmly established. The modeling of the late ($t > 10^4$ s) afterglow data favors the external forward shock model (see Piran 1999; Mészáros 2002; Zhang & Mészáros 2004, for reviews). The radiation mechanisms employed in the modeling are synchrotron radiation and synchrotron self-Compton (SSC) scattering. In the early time the prolonged activity of the central engine plays an important role in producing afterglow emission too, particularly in X-ray band (e.g., Katz et al. 1998; Fan & Wei 2005; Nousek et al. 2006; Zhang et al. 2006). The radiation mechanisms, remaining unclear, are assumed to be the same as those of the prompt soft gamma-ray emission. It is expected that in the Fermi era the origin of the prompt emission can be better understood. This is because the Large Area Telescope (LAT) and the Gamma-ray Burst Monitor (GBM) onboard Fermi satellite (<http://fermi.gsfc.nasa.gov/>) can measure the spectrum in a very

wide energy band (from 8 keV to more than 300 GeV), with which some models may be well distinguished. For example, in the standard internal shock model the SSC radiation can give rise to a distinct GeV excess while in the magnetized outflow model no GeV excess is expected.

Motivated by the detection of some > 100 MeV photons from quite a few GRBs by the Compton Gamma Ray Observatory satellite in 1991–2000 (e.g., Hurley et al. 1994; Fishman & Meegan 1995; González et al. 2003), the prompt high energy emission has been extensively investigated and most calculations are within the framework of the standard internal shocks (e.g., Pilla & Loeb 1998; Pe’er & Waxman 2004; Gupta & Zhang 2007; Bosnjak et al. 2009, cf. Giannios 2007). The detection prospect for LAT seems very promising (see Fan & Piran 2008, for a recent review).

Since the launch of Fermi satellite on 11 June 2008, significant detections of prompt high energy emission from GRBs have been only reported in GRB 080825C (Bouvier et al. 2008), GRB 080916C (Abdo et al. 2009), GRB 081024B (Omodei 2008), GRB 090323 (Ohno et al. 2009b), GRB 090328 (Cutini et al. 2009), possibly and GRB 090217 (Ohno et al. 2009a) until now (5 May 2009). Though the detection of 3 prompt photons above 10 GeV from GRB 080916C at redshift $z \sim 4.5$ (Abdo et al. 2009;

* Email: yizhong@nbi.dk

Greiner et al. 2009) is amazing and may imply a very high initial Lorentz factor of the outflow $\Gamma_i > 1800$ and an efficient acceleration of particles to very high energy (Zou et al. 2009), the non-detection of a significant > 100 MeV emission from most GRBs may be a better clue of the underlying physics. A delay in the onset of the > 100 MeV emission with respect to the soft gamma-rays, as detected in GRB 080825C, GRB 080916C, GRB 081024B and GRB 090323, may be the other clue of the GRB physics (Abdo et al. 2009; Ohno et al. 2009b). In this work we focus on these two novel observational features.

This work is structured as the following. In section 2 we discuss the constraint of the current Fermi GRB data on the standard internal shock model and several alternatives. In section 3 we look for distinguished signals in linear polarization of the prompt emission. In section 4 we briefly discuss the implication of the current Fermi results on the detection prospect of PeV neutrinos from GRBs. We summarize our results in section 5.

2 INTERPRETING THE LACK OF GEV EXCESS IN MOST GRBS AND THE DELAY OF THE ARRIVAL OF THE > 100 MEV PHOTONS

In the leading *internal shock model* for the prompt emission (Narayan et al. 1992; Paczyński & Xu 1994; Rees & Mészáros 1994; Daigne & Mochkovitch 1998), the ultra-relativistic outflows are highly variable. The faster shells ejected at late times catch up with the slower ones ejected earlier and then power energetic forward/reverse shocks at a radius $R_{\text{int}} \sim 5 \times 10^{13} (\Gamma_i/300)^2 (\delta t_\nu/10 \text{ ms}) \text{ cm}$, where Γ_i is the initial Lorentz factor of the outflow and δt_ν is the intrinsic variability timescale. Part of the shock energy has been used to accelerate electrons and part has been given to the magnetic field. If the outflow is magnetized (Usov 1992; Duncan & Thompson 1992; Lyutikov & Blandford 2003; Giannios & Spruit 2005), we call the shocks generated in the collisions within the outflow the *magnetized internal shocks* (Spruit et al. 2001; Fan et al. 2004b). The synchrotron radiation of the shock-accelerated electrons may peak in soft gamma-ray band and then account for the observed prompt emission. This model has been widely accepted for the following good reasons: (1) For an ultra-relativistic outflow moving with an initial Lorentz factor Γ_i , the velocity (in units of c) is $\beta_i = \sqrt{1 - 1/\Gamma_i^2}$. A small velocity dispersion $\delta\beta_i \sim \beta_i/(2\Gamma_i^2)$ will yield a very different Lorentz factor. As a result, internal shocks within the GRB outflow seem inevitable. (2) In the numerical simulation of the collapsar launching relativistic outflow, people found highly variable energy deposition in the polar regions in a timescale as short as ~ 50 ms (MacFadyen & Woosley 1999). (3) This model can naturally account for the variability that is well detected in prompt gamma-ray emission (Kobayashi et al. 1997). On the other hand, this model usually predicts a fast cooling spectrum $F_\nu \propto \nu^{-1/2}$ in the X-ray band. However, the data analysis finds a typical X-ray spectrum $F_\nu \propto \nu^0$ (Preece et al. 2000; Band et al. 1993). Such a divergence between the model and the observation data is the so-called ‘‘the low energy spectral index crisis’’ (Ghisellini & Celotti 1999). Another potential disadvantage of the internal shock model is its low efficiency of converting the kinetic energy of the outflow into prompt emission (e.g., Kumar 1999). Among the various solutions put forward, a plausible scenario is the *photosphere-internal shock model* (e.g., Rees & Mészáros 2005; Pe’er et al. 2006; Thompson et al. 2007). The idea is that the thermal emission leaking from the

photosphere is the dominant component of the prompt sub-MeV photons (Thompson 1994; Mészáros & Rees 2000; Ryde 2005; Ioka et al. 2007). The nonthermal high energy emission is likely the external inverse Compton (EIC) radiation of the internal shock-accelerated electrons cooled by the thermal photons from the photosphere (Rees & Mészáros 2005; Pe’er et al. 2005, 2006; Thompson et al. 2007). If the electrons are accelerated by gradual magnetic energy dissipation rather than by internal shocks, it is called the *photosphere-gradual magnetic dissipation model* (Giannios 2007). There is an increasing interest in these two kinds of models since: (1) In the spectrum analysis people did find evidences for a thermal emission component in dozens of bright GRBs (Ryde 2005; Ryde et al. 2006; Ryde & Pe’er 2009; McGlynn et al. 2009). (2) The emission from the photosphere can naturally account for the temporal behaviors of the temperature and flux of these thermal radiation (Pe’er 2008). (3) The overall spectrum of the prompt emission can be reasonably interpreted (e.g., Pe’er et al. 2006; Giannios 2007). (4) The GRB efficiency can be much higher than that of the internal shock model (see Ryde & Pe’er 2009, and the references therein).

In this section we test these four models with the current Fermi GRB data. It is somewhat surprisingly to see that none of these models have been ruled out.

2.1 Explaining the lack of GeV spectrum excess in most GRBs

2.1.1 The standard internal shock model

In this model, the outflow is baryonic and the thermal emission during the initial acceleration of the outflow is ignorable. The prompt emission is powered by energetic internal shocks. There are three basic assumptions. (i) ϵ_e , ϵ_B , ϵ_p fractions of shock energy have been given to electrons, magnetic field and protons, respectively (note that $\epsilon_e + \epsilon_B + \epsilon_p = 1$). (ii) The energy distribution of the shock-accelerated electrons is a single power-law. (iii) The prompt soft gamma-ray emission is attributed to the synchrotron radiation of the shocked electrons.

For internal shocks generating at R_{int} , the typical random Lorentz factor of the electrons can be estimated as (see section 4.1.1 of Fan & Piran (2008) for details)

$$\gamma'_{e,m} \sim 760 (1 + Y_{\text{SSC}})^{1/4} L_{\text{syn},52}^{-1/4} R_{\text{int},13}^{1/2} (1+z)^{1/2} (\epsilon_p/300 \text{ keV})^{1/2}, \quad (1)$$

where $\epsilon_p = h\nu_m$ is the observed peak energy of the synchrotron-radiation spectrum (νF_ν), h is the Planck’s constant, L_{syn} is the synchrotron-radiation luminosity of the internal shock emission, $Y_{\text{SSC}} \sim [-1 + \sqrt{1 + 4\epsilon_e/(1 + g^2)\epsilon_B}]/2$ is the regular SSC parameter (Sari & Esin 2001; Fan & Piran 2008; Piran et al. 2009), and $g \sim \gamma'_{e,m}\epsilon_p/\Gamma_i m_e c^2$. The SSC in the extreme Klein-Nishina regime ($g \gg 1$) is very inefficient. If that happens the non-detection of GeV spectrum excess in most Fermi GRBs can be naturally explained. With the typical parameters adopted in eq.(1) we have $g \sim 1$, for which the SSC may still be important (i.e., $Y_{\text{SSC}} \geq 1$). In this work the convenience $Q_x = Q/10^x$ has been adopted in cgs units except for some specific notations.

The SSC radiation will peak at

$$h\nu_{m,\text{SSC}} \sim \frac{2\gamma_{e,m}^2 \epsilon_p}{1 + 2g} \sim 220 \text{ GeV} (1 + 2g)^{-1} (1 + Y_{\text{SSC}})^{1/2} L_{\text{syn},52}^{-1/2} R_{\text{int},13} (1+z) (\epsilon_p/300 \text{ keV})^2. \quad (2)$$

Taking into account the energy loss of the electrons via in-

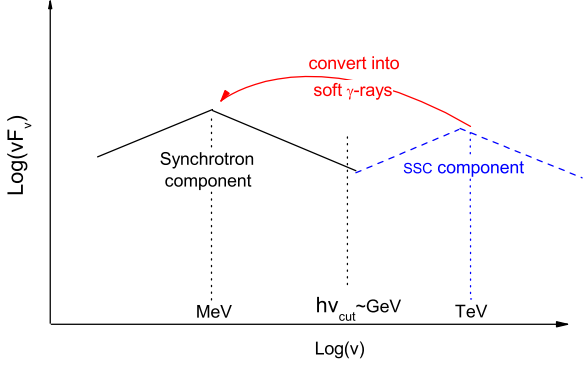


Figure 1. A possible interpretation of the non-detection of the SSC component by Fermi satellite in the internal shock model. The high energy photons with an energy $> h\nu_{\text{cut}}$ have been absorbed by the soft gamma-rays and energetic e^\pm pairs are formed. The pairs will lose their energy through synchrotron radiation and/or inverse Compton scattering and then produce soft gamma-rays.

verse Compton scattering on prompt soft gamma-rays, the cooling Lorentz factor can be roughly estimated as

$$\gamma'_{e,c} \sim 0.03 L_{\text{syn},52}^{-1} R_{\text{int},13} \Gamma_{2.5}^3. \quad (3)$$

In reality $\gamma'_{e,c}$ is always larger than 1. The derived $\gamma'_{e,c} < 1$ just means that the electrons have lost almost all their energies and are sub-relativistic.

Prompt high energy photons above the cut-off frequency ν_{cut} will produce pairs by interacting with softer photons and will not escape from the fireball. Following Lithwick & Sari (2001) and Fan & Piran (2008), we have

$$h\nu_{\text{cut}} \approx 2 \text{ GeV} (1+z)^{-1} (\epsilon_p/300 \text{ keV})^{(2-p)/p} L_{\text{syn},52}^{-2/p} \delta t_{v,-2}^{2/p} \Gamma_{i,2.5}^{(2p+8)/p}. \quad (4)$$

The SSC radiation spectra can be approximated by $F_{\nu_{\text{SSC}}} \propto \nu^{-1/2}$ for $\nu_{\text{m}} < \nu < \nu_{\text{m,SSC}}$, and $F_{\nu_{\text{SSC}}} \propto \nu^{-p/2}$ ($F_{\nu_{\text{SSC}}} \propto \nu^{-p}$) for $\nu > \nu_{\text{m,SSC}}$ and $g \leq 1$ ($g \gg 1$). The energy ratio of the SSC radiation emitted below ν_{cut} to the synchrotron radiation in the energy range $\nu_{\text{m}} < \nu < \max\{\nu_{\text{M}}, \nu_{\text{cut}}\}$ can be estimated as

$$\mathcal{R} \sim \frac{Y_{\text{SSC}} \nu_{\text{m}}^{(2-p)/2} \int_{\nu_{\text{m}}}^{\nu_{\text{cut}}} \nu^{-1/2} d\nu}{\nu_{\text{m,SSC}}^{1/2} \int_{\nu_{\text{m}}}^{\max\{\nu_{\text{M}}, \nu_{\text{cut}}\}} \nu^{-p/2} d\nu} \approx (p-2) (\nu_{\text{cut}}/\nu_{\text{m,SSC}})^{1/2} Y_{\text{SSC}}, \quad (5)$$

where $\nu_{\text{M}} \approx 30 \Gamma_i (1+z)^{-1} \text{ MeV}$ is the maximal synchrotron radiation frequency of the shocked electrons (Cheng & Wei 1996).

For $Y_{\text{SSC}} \sim 1$, $p \sim 2.5$ (corresponding to the typical γ -ray spectrum $F_\nu \propto \nu^{-1.25}$ for $h\nu > \epsilon_p$) and $\nu_{\text{cut}} \ll \nu_{\text{m,SSC}}$, we have $\mathcal{R} \ll 1$. Therefore there is no GeV excess in the spectrum, in agreement with the data. In other words, the non-detection of a significant high energy component is due to a too large $h\nu_{\text{m,SSC}} \sim \text{TeV}$ and a relative low $h\nu_{\text{cut}} \sim \text{GeV}$ (see Fig.1 for a schematic plot). The other possibility is that $(1+g^2)\epsilon_B > 4\epsilon_e$, for which $Y_{\text{SSC}} \sim \mathcal{O}(1)$, i.e., the SSC radiation is unimportant and can be ignored.

2.1.2 The photosphere–internal shock model

Thompson (1994) proposed the first photosphere model for the prompt gamma-ray emission, in which the nonthermal X-ray and gamma-ray emission are attributed to the Compton upscattering of the thermal emission by the mildly relativistic Alfvén turbulence. The spectra of GRBs can be nicely reproduced (see also Pe’er et al. 2006; Giannios 2007). It is, however, difficult to explain the energy dependence of the width of the gamma-ray pulse (Fenimore et al. 1995; Norris et al. 1996). As shown in Thompson et al. (2007), such a puzzle may be solved in the photosphere–internal shocks model, in which the sub-MeV emission is dominated by the thermal emission of the fireball and the nonthermal tail is the EIC radiation of the electrons accelerated in internal shocks at a radius $R_{\text{int}} \sim 10^{14} \text{ cm}$ (e.g., Mészáros & Rees 2000; Rees & Mészáros 2005; Pe’er et al. 2006). In this model the shock accelerated electrons take a power-law energy distribution $dn/d\gamma'_e \propto \gamma'^{-p}$ for $\gamma'_e \geq \gamma'_{e,m} \sim 1$. Such an initial distribution can not keep if the electrons cool down rapidly. As shown in Sari et al. (1998), in the presence of steady injection of electrons, the energy distribution can be approximated by $N_{\gamma_e} \propto \gamma'^{-(p+1)}$ for $\gamma'_e > \max\{\gamma'_{e,c}, \gamma'_{e,m}\}$ and $N_{\gamma_e} \propto \gamma'^{-2}$ for $\gamma'_{e,c} < \gamma'_e < \gamma'_{e,m}$. Under what conditions can shock acceleration generate a particle distribution with $\gamma'_{e,m} \sim 1$, with a significant fraction of the outflow energy deposited in the nonthermal particles? There could be two ways. One is to assume that electron/positron pair creation in the outflow is so significant that the resulting pairs are much more than the electrons associated with the protons. As a result, the fraction of shock energy given to each electron/positron will be much smaller than that in the case of a pair-free outflow and a $\gamma'_{e,m} \sim 1$ is achievable (Thompson et al. 2007). The other way is to assume that the particle heating is continuous. In the internal shock scenario, this could happen if an outflow shell consists of many sub-shells and the weak interaction between these sub-shells may be able to produce multiple shocks that can accelerate electrons continually with a very small $\gamma'_{e,m}$.

Since both $\gamma'_{e,m}$ and $\gamma'_{e,c}$ are ~ 1 , the EIC spectrum should be $F_\nu \propto \nu^{-p/2}$ in the MeV-TeV energy range and there is no GeV excess for $p \sim 2.5$, consistent with the Fermi data.

2.1.3 The magnetized internal shock model

If the unsteady GRB outflow carries a moderate/small fraction of magnetic field, the collision between the fast and slow parts will generate strong internal shocks and then produce energetic soft gamma-ray emission. As usual, the ratio between the magnetic energy density and the particle energy density is denoted as σ . In the ideal MHD limit, for $\sigma \gg 1$ just a very small fraction of the upstream energy can be converted into the downstream thermal energy. Therefore the GRB efficiency is very low¹. That’s why peo-

¹ For the Poynting-flux dominated outflow (i.e., $\sigma \gg 1$), Usov (1994) proposed that at the radius $r_{\text{MHD}} \sim 6 \times 10^{15} L_{52}^{1/2} \sigma_2^{-1} t_{v,m-3} \Gamma_{i,2.5}^{-1} \text{ cm}$, the MHD condition breaks down and large scale electromagnetic waves are generated, where L is the total luminosity of the outflow and $t_{v,m}$ is the minimum variability timescale of the central engine (see also Zhang & Mészáros 2002). The particles are accelerated and the synchrotron radiation of the ultra-relativistic electrons peaks at $\nu_{\text{m}} \sim 5 \times 10^{19} \sigma_2^3 (\epsilon_e/0.2)^2 [3(p-2)/(p-1)]^2 \Gamma_{2.5} t_{v,m-3} \text{ Hz}$ (Fan et al. 2005), provided that a significant part of the magnetic energy has been converted to the thermal energy of the particles. In this scenario, the SSC radiation is expected to be very weak because in the rest frame of the electrons having $\gamma'_{e,m} \sim 10^4 (\epsilon_e/0.2) [3(p-2)/(p-1)] \sigma_2$ (Fan et al. 2005), the soft

ple concentrate on the internal shocks with a magnetization $\sigma \leq 1$ (Spruit et al. 2001; Fan et al. 2004b).

For the magnetized internal shocks with $\sigma \geq 0.1$, no significant high energy emission is expected since: (a) The SSC emission of the internal shocks is weak. Therefore there is no distinct GeV excess in the spectrum. (b) The synchrotron-radiation spectrum may be very soft, which renders the detection of GeV photons from GRBs more difficult. The reason is the following. For an isotropic diffusion and a relativistic shock, the electron energy distribution index can be estimated by (Keshet & Waxman 2005)

$$p \sim (3\beta_u - 2\beta_u\beta_d^2 + \beta_d^3)/(\beta_u - \beta_d) - 2. \quad (6)$$

However, in the presence of a large scale coherent magnetic field, the diffusion is highly anisotropic rather than isotropic (Morlini et al. 2007a). There are thus corrections to eq.(6). But as long as the scattering is not very forward- or backward-peaked, these corrections are small (Keshet 2006). Taking into account the anisotropic correction, Morlini et al. (2007b) found a spectrum steep to $p \sim 3$ for $\sigma \sim 0.05$. In the ion-electron shock simulation, the acceleration of particles at the un-magnetized shock front is a lot more efficient than that with a $\sigma \sim 0.1$ (Sironi & Spitkovsky 2009). Motivated by these two possible evidences, we adopt eq.(6) to estimate the spectral slope of accelerated particles at the magnetized shock fronts. The validity of our approach can be tested by the advanced numerical simulations in the future.

In the case of $\sigma = 0$, for an ultra-relativistic shock, $\beta_u \rightarrow 1$ and $\beta_d \rightarrow 1/3$, we have $p \rightarrow 2.22$. But for an ultra-relativistic magnetized shock, $\beta_u \rightarrow 1$ and (e.g., Fan et al. 2004b)

$$\beta_d \approx \frac{1}{6}(1 + \chi + \sqrt{1 + 14\chi + \chi^2}), \quad (7)$$

where $\chi \equiv \sigma/(1 + \sigma)$, please note that σ is measured in the upstream. Note in this work we just discuss the ideal MHD limit, i.e., there is no magnetic energy dissipation at the shock front. For $0 < \sigma \leq 1$, we have $p \sim (4.22 - 2\sigma)/(1 - 2\sigma) - 2 > 2.22$. For $\sigma \gg 1$, we have $\beta_d \rightarrow 1 - 1/2\sigma$ and $p \sim 4\sigma - 1 \gg 2.22$. Correspondingly, the electron spectrum is very soft or even thermal-like. Adopting $\beta_u \sim 1$ and substituting $\sigma \sim (1, 0.5, 0.1, 0.01)$ into eqs.(6-7), we have $p \sim (6.6, 4.5, 2.7, 2.3)$. The (very) soft high energy spectra of some GRBs (e.g., Preece et al. 2000, see also our Fig.2 for the Fermi GRBs) may be interpreted in this way.

If the weak prompt high energy emission of GRBs is indeed attributed to the magnetization of the outflow, one can expect that the smaller the p , the stronger the high energy emission. The ongoing analysis of the LAT data will test such a correlation.

2.1.4 The photosphere—gradual magnetic dissipation model

Giannios (2007) calculated the emission of a Poynting-flux-dominated GRB outflow with gradual magnetic energy dissipation (reconnection). In his scenario, the energy of the radiating electrons is determined by heating and cooling balance. The mildly relativistic electrons stay thermal throughout the dissipation region because of Coulomb collisions (Thomson thick part of the flow) and exchange of synchrotron photons (Thomson thin part). Rather similar to Thompson (1994), the resulting spectrum naturally explains

gamma-rays have an energy $\gamma'_{e,m} h\nu_m/\Gamma_i \gg m_e c^2$, i.e., the SSC is in the extreme Klein-Nishina regime and is very inefficient. The non-detection of high energy emission from most GRBs is, of course, consistent with this model.

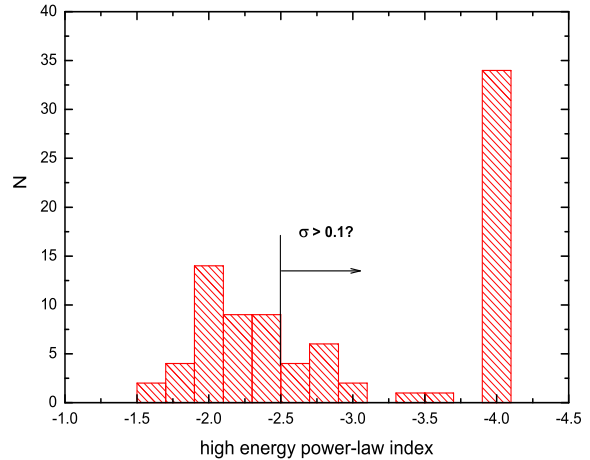


Figure 2. The distribution of the high energy power-law index (β_{Band}) of GRBs detected by Fermi satellite from 10 August 2008 to 31 March 2009. The data are taken from <http://www.batsf.msfc.nasa.gov/gbm/circulars/> (see also http://gcn.gsfc.nasa.gov/gcn3_archive.html) and are preliminary. The GRBs having a single power-law spectrum in the GBM energy range are excluded in the statistics. Following Preece et al. (2000) we take $\beta_{\text{Band}} = -4$ for all bursts that can be better fitted by a power-law function with an exponential high energy cutoff rather than by the Band function (Band et al. 1993). We find that a good fraction of bursts have a $p \sim -2(\beta_{\text{Band}} + 1) > 2.22$, consistent with Preece et al. (2000). These soft spectra may be attributed to the magnetized internal shocks.

the observed sub-MeV break of the GRB emission and the spectral slopes. In this scenario, different from the magnetized internal shock model, the higher the initial σ , the harder the spectrum (see the Fig.2 of Giannios (2007) for illustration). For an initial $\sigma \leq 40$ (corresponding to the baryon loading $L/\dot{M}c^2 \sim \sigma^{3/2} \leq 250$, where \dot{M} is the mass loading rate), the resulting > 10 MeV spectrum is very soft (see also Drenkhahn 2002; Drenkhahn & Spruit 2002), accounting for the failed detection of the GeV spectrum excess in most GRBs.

2.2 Interpreting the delay of the arrival of the > 100 MeV photons

In both the collapsar and the compact star merger models for GRBs (see Piran 1999; Mészáros 2002; Zhang & Mészáros 2004, for reviews), the early outflow may suffer more serious baryon pollution and thus have a smaller Γ_i than the late ejecta (Zhang, Woosley & MacFadyen 2004). This may explain the delay of the arrival of the > 100 MeV emission since as long as

$$\Gamma_i \leq \Gamma_{i,c} = 180(1+z) \frac{v}{2p+8} \left(\frac{h\nu_{\text{cut}}}{100 \text{ MeV}} \right)^{\frac{p}{2p+8}} \left(\frac{\varepsilon_p}{300 \text{ keV}} \right)^{\frac{p-2}{2p+8}} L_{\text{syn},52}^{\frac{1}{4+p}} \delta t_{v,-2}^{-\frac{1}{4+p}},$$

the > 100 MeV photons can not escape from the emitting region freely and thus can not be detected.

In the photosphere-gradual magnetic dissipation model, a small Γ_i implies a low initial magnetization of the outflow, for which the high energy spectrum can be very soft (Drenkhahn & Spruit 2002; Giannios 2007). In the magnetized internal shock model, the delay of the onset of the LAT observation indicates a larger magnetization of the early internal shocks if $\Gamma_i > \Gamma_{i,c}$.

In the collapsar scenario, before the breakout, the initial outflow is choked by the envelope material of the massive star (Zhang

et al. 2004). The ultra-relativistic reverse shock may be able to smooth out the velocity/energy-density dispersion of the initial ejecta. So the internal shocks generated within the early/breakout outflow may be too weak to produce a significant non-thermal radiation component. The early emission is then dominated by the thermal component from the photosphere and may last a few seconds (provided that the choked material has a width comparable to that of the envelope of the progenitor). The outflow launched after the breakout of the early ejecta can escape from the progenitor freely and the consequent internal shocks can be strong enough to produce energetic non-thermal radiation. The photosphere-internal shock model therefore might be able to naturally account for the delay in the onset of the LAT observation.

In summary, before and after the onset of the > 100 MeV emission, it seems the physical properties of the outflow have changed.

3 THE LINEAR POLARIZATION SIGNAL OF THE PROMPT γ -RAY EMISSION

As discussed in section 2, the failed detection of the GeV spectrum excess in most GRBs can be understood in either the standard internal shock model or several alternatives. Therefore we need independent probes to distinguish between these scenarios. Our current purpose is to see whether the polarimetry in gamma-ray band can achieve such a goal. In this section, we firstly investigate the linear polarization property of the photosphere-internal shock model (*the results may apply to the photosphere-gradual magnetic dissipation model as well*) since it has not been reported by others yet². We then briefly discuss the linear polarization signals expected in the magnetized internal shock model and in the standard internal shock model since they have been extensively discussed in the literature (e.g., Lyutikov et al. 2003; Granot 2003; Waxman 2003; Nakar et al. 2003; Fan et al. 2008; Toma et al. 2009).

3.1 Linear polarization signal of the photosphere-internal shock model

In this work we assume an uniform outflow. At any point in the outflow there is a preferred direction, the radial direction, in which the fluid moves. We choose the Z' -direction of the fluid local frame coordinate to be in that direction. The Y' -direction is chosen to be within the plane containing the line of sight (i.e., the scattered photon k'_o) and the Z' -axis (see Fig.3). In this frame, the incident photons (k') are along the Z' -direction.

As usual, we assume that the electrons are isotropic in the co-moving frame of the emitting region³. The incident photons are the thermal emission from the photosphere and are unpolarized.

² In the final stage of preparing the manuscript, the author was informed by K. Toma and X. F. Wu that the POET (Polarimeters for Energetic Transients) group discussed the polarization property of the photosphere-internal shock model independently. The preliminary results were included in their white paper.

³ In the current scenario, the electrons are heated by the internal shocks and an isotropic distribution in the rest frame of the emitting region may be a good approximation. Such a distribution, however, will be modified by the cooling of the electrons via EIC scattering on the thermal photons from the inner part of the outflow. Detailed numerical simulation is needed to see such a modification and then its influence on the inverse Compton radiation, which is beyond the scope of this work.

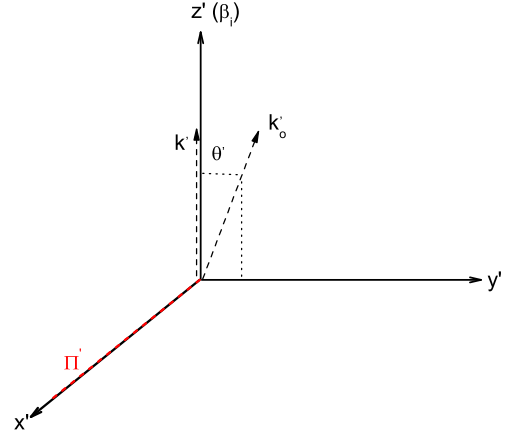


Figure 3. The coordinates in the comoving frame of the emitting region. The polarization vector $\hat{\Pi}'$ is along the X' -direction for a positive P given in eq.(11) otherwise it would be along $\hat{X}' \times \hat{k}'_o$.

The energy of the incident and the scattered photons are $h\nu'_{se}$ and $h\nu'$, respectively. As shown in Aharonian & Atoyan (1981) and Berestetskii et al. (1982): (I) In the cloud of the isotropic electrons of energies $\gamma'_e m_e c^2$, the spectrum of photons, upscattered at the angle θ' relative to the direction of the seed photon beam, can be approximated by

$$\frac{dN_\gamma}{dt d\nu' d\Omega'} \approx \frac{3\sigma_{TC} n_{\nu'_{se}} d\nu'_{se}}{16\pi\gamma_e'^2 \nu'_{se}} \frac{x}{2\beta_e' Q} (4A_0^2 - 4A_0 + B_0), \quad (8)$$

where $\beta_e' = (1 - 1/\gamma_e'^2)^{-1/2}$ and

$$A_0 = \frac{1}{2\delta\gamma_e'^2 x} \left(\frac{1}{\mathcal{T}_1} - \frac{1}{\mathcal{T}_2} \right),$$

$$B_0 = \frac{\mathcal{T}_2}{\mathcal{T}_1} + \frac{\mathcal{T}_1}{\mathcal{T}_2},$$

$$\mathcal{T}_1 = (1 - \cos\theta') \frac{1 + x + x\delta \cos\theta' - \delta x^2}{Q^2},$$

$$\mathcal{T}_2 = (1 - \cos\theta') \frac{1 + x - x\delta \cos\theta' + \delta}{Q^2},$$

$$Q \equiv \sqrt{1 + x^2 - 2x \cos\theta'},$$

$$\delta \equiv h\nu'_{se}/(\gamma'_e m_e c^2), \quad x \equiv \nu'/\nu'_{se}. \quad (9)$$

Please note that x ranges from x_m to x_M that are given by

$$x_{m,M} = 1 + \frac{\{\mathcal{A} \mp \gamma'_e \beta_e' \sqrt{\gamma_e'^2 (1 + \delta)^2 (1 - \cos\theta')^2 + \sin^2\theta'}\}}{1 + 2\delta\gamma_e'^2 (1 - \cos\theta') + \gamma_e'^2 \delta^2 (1 - \cos\theta')^2}, \quad (10)$$

where $\mathcal{A} \equiv (1 - \cos\theta')\gamma_e'^2 [\beta_e'^2 - \delta - \delta^2 (1 - \cos\theta')]$.

(II) The polarization degree is

$$P \approx \frac{4(A_0 - A_0^2)}{B_0 - 4A_0 + 4A_0^2}. \quad (11)$$

For the relativistic electrons (i.e., $\beta_e \rightarrow 1$), eq.(8) and eq.(11) take the simplified forms

$$\begin{aligned} \frac{dN_\gamma}{dt d\nu' d\Omega'} &\approx \frac{3\sigma_{TC} n_{\nu'_{se}} d\nu'_{se}}{16\pi\gamma_e'^2 \nu'_{se}} \left[1 + \frac{\xi^2}{2(1-\xi)} - \frac{2\xi}{b_\theta(1-\xi)} \right. \\ &\quad \left. + \frac{2\xi^2}{b_\theta^2(1-\xi)^2} \right], \end{aligned} \quad (12)$$

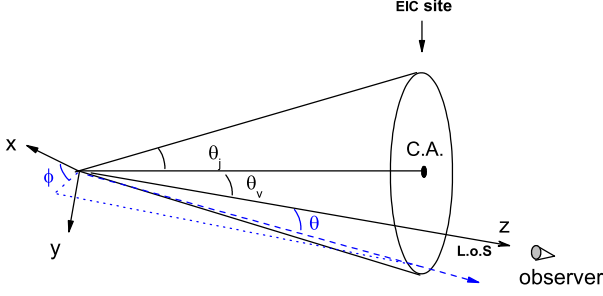


Figure 4. Sketch of the geometrical set-up used to compute the polarization signal. We take the L.o.S as the z -axis. The y -axis (x -axis) is within (perpendicular to) the plane containing the line of sight and central axis of the ejecta.

$$P \approx \frac{\frac{2\xi}{b_\theta(1-\xi)} - \frac{2\xi^2}{b_\theta^2(1-\xi)^2}}{1 + \frac{\xi^2}{2(1-\xi)} - \frac{2\xi}{b_\theta(1-\xi)} + \frac{2\xi^2}{b_\theta^2(1-\xi)^2}}, \quad (13)$$

where $\xi \equiv h\nu' / (\gamma'_e m_e c^2)$, $b_\theta = 2(1 - \cos \theta') \gamma'_e h\nu'_{se} / (m_e c^2)$, and $h\nu'_{se} \ll h\nu' \leq \gamma'_e m_e c^2 b_\theta / (1 + b_\theta)$.

Since the emitting region is moving relativistically, the angle θ' (in Fig.3) corresponding to the line of sight (L.o.S) is given by

$$\cos \theta' = (\cos \theta - \beta_i) / (1 - \beta_i \cos \theta), \quad (14)$$

where θ is the angle between the line of sight and the emitting point (measured in the observer's frame).

The azimuthal angle ϕ varying from 0 to 2π is defined in Fig.4. The polar angle θ ranges from 0 to $\theta_v + \theta_j$. The angle between the vector $(\sin \theta \cos \phi, \sin \theta \sin \phi, \cos \theta)$ and the central axis of the ejecta (C.A. in Fig.4) is denoted as Θ and is given by

$$\cos \Theta = -\sin \theta_v \sin \theta \sin \phi + \cos \theta_v \cos \theta. \quad (15)$$

Please *bear in mind* that in the following radiation calculation, the flux is set to be zero if $\cos \Theta < \cos \theta_j$ because these points (θ, ϕ) are outside of the cone of the ejecta.

The EIC radiation flux in the observer frame is

$$F_{\nu, \text{EIC}} \propto \int \mathcal{D}^3 h\nu' \frac{dN_\gamma}{dt d\nu' d\Omega'} N_{\gamma_e} d\gamma'_e d\Omega, \quad (16)$$

where $\nu = \mathcal{D}\nu' / (1 + z)$, $\mathcal{D} = [\Gamma_i (1 - \beta_i \cos \theta)]^{-1}$ is the Doppler factor, and Ω is the solid angle satisfying $d\Omega = \sin \theta d\theta d\phi$.

The polarized radiation flux is

$$Q_{\nu, \text{EIC}} \propto \int \mathcal{D}^3 h\nu' P \cos 2\phi \frac{dN_\gamma}{dt d\nu' d\Omega'} N_{\gamma_e} d\gamma'_e d\Omega. \quad (17)$$

The polarization degree of the EIC emission is

$$P_{\nu, \text{EIC}} = |Q_{\nu, \text{EIC}}| / F_{\nu, \text{EIC}}. \quad (18)$$

One can see that a non-zero net polarization is expected as long as $\theta_v > 0$. In the numerical example, we assume that the seed photons have a thermal spectrum (as suggested in the photosphere model)

$$n_{\nu'_{se}} \propto \frac{(h\nu'_{se})^2}{e^{h\nu'_{se}/kT'} - 1}, \quad (19)$$

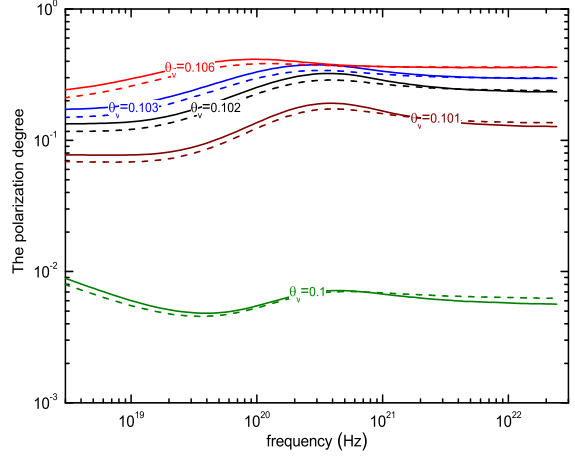


Figure 5. The degree of the linear polarization of the EIC component as a function of frequency. The half-opening angle of the ejecta θ_j and the bulk Lorentz factor Γ_i are assumed to be 0.1 and 300, respectively. The viewing angle θ_v is marked in the plot. The solid and dashed lines are for the electron distribution $N_{\gamma_e} \propto \gamma_e'^{-3.5}$ and $N_{\gamma_e} \propto \gamma_e'^{-2}$, respectively.

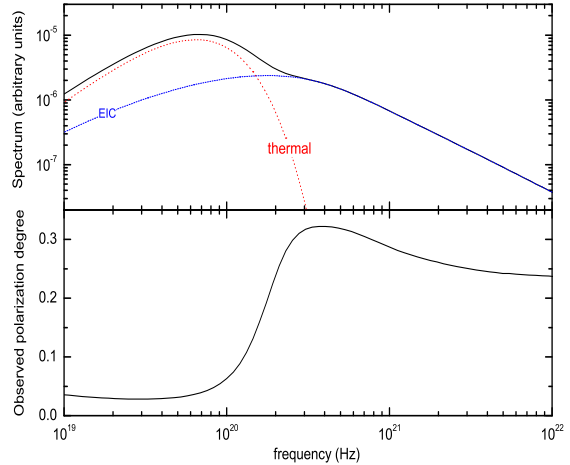


Figure 6. The spectrum of one simulated GRB (the upper panel) and the expected linear polarization degree of the total emission as a function of the photon energy (the lower panel). In the calculation we take $\theta_v = 0.102$. Other parameters are the same as those used in Fig.6 in the case of $N_{\gamma_e} \propto \gamma_e'^{-3.5}$.

where $kT' \approx kT/2\Gamma_i$ is the temperature (measured in the rest frame of the emitting region) of the thermal emission. In the calculation we take $\Gamma_i \sim 300$ and $kT \sim 100$ keV. The electron distribution is taken as $N_{\gamma_e} \propto \gamma_e'^{-(1+p)} \propto \gamma_e'^{-3.5}$ for $\gamma_e' > 2$, otherwise $N_{\gamma_e} = 0$. For comparison purpose we also consider the case of $N_{\gamma_e} \propto \gamma_e'^{-2}$. The numerical results are presented in Fig.5. One can see that the polarization degrees expected in these two representative cases are only slightly different. We also find that a moderate linear polarization level ($P_{\nu, \text{EIC}} > 10\%$) is achievable only for $\theta_v \gtrsim \theta_j + 1/(3\Gamma_i)$.

Currently the prompt emission consists of a thermal and a non-

thermal components. The thermal component with the flux $F_{\nu,\text{th}}$ is expected to be unpolarized while the nonthermal EIC component may have a high linear polarization level. The observed polarization degree

$$P_{\nu,\text{obs}} = \frac{|Q_{\nu,\text{EIC}}|}{F_{\nu,\text{EIC}} + F_{\nu,\text{th}}}$$

should be strongly frequency-dependent. Roughly speaking, the linear polarization degree is anti-correlated with the weight of the thermal component. With an energy $\sim kT$, the emission is dominated by the thermal component and $P_{kT,\text{obs}}$ is low. For $h\nu \gg kT$, the emission is dominated by the EIC component and $P_{\nu,\text{obs}} \sim P_{\nu,\text{EIC}}$, as illustrated in Fig.6. This unique behavior⁴ can help us to distinguish it from other models.

The probability of detecting a moderate/high linear polarization degree (\mathcal{R}_{pol}), however, is not high (Please note that we do not take into account the weak events for which a reliable polarimetry is impossible). On the one hand, a high linear polarization level is achievable only for $\theta_\nu \geq \theta_j + 1/3\Gamma_i$. On the other hand, $\theta_\nu - \theta_j \lesssim 1/\Gamma_i$ is needed otherwise the burst will be too weak to perform the gamma-ray polarimetry. For $\Gamma_i\theta_j \gg 1$, we have

$$\mathcal{R}_{\text{pol}} \sim 4/(3\Gamma_i\theta_j) \approx 5\% \Gamma_{i,2.5}^{-1} \theta_{j,-1}^{-1}. \quad (20)$$

During the revision of this work, McGlynn et al. (2009) reported their analysis on the spectrum and the polarization properties of GRB 061122. They found out that the spectrum was better fitted by the superposition of a thermal and a non-thermal components and the photons in the “thermal” emission dominated energy range had a (much) lower polarization level than those in the higher energy band. These two characters are in agreement with the photosphere-internal shock model (or the photosphere-gradual magnetic dissipation model).

3.2 Linear polarization level expected in the standard internal shock model

In the standard internal shock model, the polarization of the synchrotron radiation depends on both the *poorly known* configuration of magnetic field generated in internal shocks and the geometry of the visible emitting region. Assuming a random magnetic field that remains planar in the plane of the shock, Waxman (2003) and Nakar et al. (2003) showed that a high linear polarization level can be obtained when a narrow jet is observed from the edge, like in the photosphere-internal shock model. For the jets on-axis ($\theta_\nu \leq \theta_j$), the linear polarization degree is low (see also Gruzinov 1999 and Toma et al. 2009). The detection probability of a moderate/high linear polarization degree can also be estimated by eq.(20).

3.3 High linear polarization degree expected in the magnetized internal shock model

For the magnetized internal shock model, the prompt soft γ -ray emission is attributed to the synchrotron radiation of the electrons in ordered magnetic field and a high linear polarization level

⁴ For the synchrotron radiation of the electrons moving in a random magnetic field (the standard internal shock model) or in an ordered magnetic field (e.g., the magnetized internal shock model), before and after the peak of the spectrum, the polarization degree changes because the polarization properties depend on the profile of the spectrum. However, such a dependence is weak, as shown in Granot (2003).

Table 1. Distinguish between the models with the polarimetry data.

model	unique polarization property	\mathcal{R}_{pol}
standard internal shocks		$\lesssim 10\%$
photosphere-internal shocks [†]	strongly frequency-dependent [‡]	$\lesssim 10\%$
magnetized internal shocks		$\sim 100\%$

[†]In the photosphere-gradual magnetic dissipation model, very similar polarization properties are expected.

[‡]As shown in Fig.6, the polarization degree is anti-correlated with the weight of the photosphere/thermal component.

is expected (Lyutikov et al. 2003; Granot 2003). The physical reason is the following. The magnetic fields from the central engine are likely frozen in the expanding shells. The toroidal magnetic field component decreases as R^{-1} , while the poloidal magnetic field component decreases as R^{-2} . At the radius of the “internal” energy dissipation (or the reverse shock emission), the frozen-in field is dominated by the toroidal component. For an ultra-relativistic outflow, due to the relativistic beaming effect, only the radiation from a very narrow cone (with the half-opening angle $\leq 1/\Gamma_i$) around the line of sight can be detected. As long as the line of sight is off the symmetric axis of the toroidal magnetic field, the orientation of the viewed magnetic field is nearly the same within the field of view. The synchrotron emission from such an ordered magnetic field therefore has a preferred polarization orientation (i.e. perpendicular to the direction of the toroidal field and the line of sight). Consequently, the linear polarization of the synchrotron emission of each electrons could not be effectively averaged out and the net emission should be highly polarized. The detection prospect of a high linear polarization degree is very promising (i.e., $\mathcal{R}_{\text{pol}} \sim 100\%$). The above argument applies to the reverse shock emission as well if the outflow is magnetized (Fan et al. 2004a).

As summarized in Tab.1, for the magnetized internal shock model, a high linear polarization level should be typical, while for two other models a moderate/high linear polarization degree is still possible but much less frequent. So the statistical analysis of the GRB polarimetry results may be able to distinguish the magnetized internal shock model from the others (see also Toma et al. 2009). In the photosphere-internal shock model the polarization degree is expected to be strongly frequency-dependent. Such a remarkable behavior, if detected, labels its physical origin.

Indeed there were some claims of the detection of high linear polarization degree in the soft γ -ray emission of GRB 021206 (Coburn & Boggs 2003, however see Rutledge & Fox 2004), GRB 930131, GRB 960924 (Willis et al. 2005), GRB 041219A (McGlynn et al. 2007; Gotz et al. 2009), and GRB 061122 (McGlynn et al. 2009). These results are consistent with each other as the errors are very large. The situation is inconclusive and additional data is needed to test these results. Measuring polarization is of growing interest in high energy astronomy. New technologies are being invented, and several polarimeter projects are proposed, such as, in the gamma-ray band, there are the Advanced Compton Telescope Mission (Boggs et al. 2006), POET (Hill et al. 2008) and others (see Toma et al. 2009, for a summary). So in the next decade reliable polarimetry of GRBs in gamma-ray band may be realized and we can impose tight constraint on the models. At present, the most reliable polarimetry is in UV/optical band (e.g.,

Covino et al. 1999; Wijers et al. 1999). The optical polarimetry of the prompt emission and the reverse shock emission require a quick response of the telescope to the GRB alert. This is very challenging. Mundell et al. (2007) reported the optical polarization of the afterglow, at 203 sec after the initial burst of γ -rays from GRB 060418, using a ring polarimeter on the robotic Liverpool Telescope. Their robust (90% confidence level) upper limit on the percentage of polarization, less than 8%, coincides with the fireball deceleration time at the onset of the afterglow. Such a null detection is, however, not a surprise because for this particular burst the reverse shock emission is too weak to outshine the unpolarized forward shock emission (Jin & Fan 2007). Quite recently, the robotic Liverpool Telescope performed the polarimetry measurement of the reverse shock emission of GRB 090102 (Kobayashi 2009, private communication). Following Fan et al. (2002), Zhang et al. (2003) and Kumar & Panaitescu (2003), it is straightforward to show that the reverse shock of GRB 090102 is magnetized. Consequently the optical flash is expected to be highly polarized. If confirmed in the ongoing data analysis, the magnetized outflow model for some GRBs will be favored.

4 IMPLICATION ON THE DETECTION PROSPECT OF PEV NEUTRINO EMISSION

The site of the prompt γ -ray emission may be an ideal place accelerating protons to ultra-high energy (Vietri 1995; Waxman 1995). These energetic protons can produce high-energy neutrinos via photomeson interaction, mainly through Δ -resonance (Waxman & Bahcall 1997). The resulting neutrinos have a typical energy $E_{\nu, \text{obs}} \sim 5 \times 10^{14}$ eV $\Gamma_{2.5}^2 [(1+z)^2 \epsilon_{\gamma, \text{obs}} / 1 \text{ MeV}]^{-1}$. Significant detections are expected if GRBs are the main source of ultra-high energy cosmic rays (Waxman & Bahcall 1997). The underlying assumption is that the proton spectrum is not significantly softer than $dN/dE \propto E^{-2}$. The current Fermi observations do not provide an observational evidence for such a flat particle spectrum. Below we discuss the detection prospect of PeV neutrinos implicated by the non-detection of high energy emission from most GRBs. In the magnetized outflow model, the acceleration of a significant part of protons to energies $\geq 10^{16}$ eV is highly questionable because of the resulting soft proton spectrum. In the photosphere-internal shock model, $\gamma'_{e, \text{m}} \sim 1$ is needed (Thompson et al. 2007). The efficiency of accelerating protons to very high energy depends on the mechanism of the particle heating. For example, in the case of multiple internal shocks, each pair of internal shocks are expected to be very weak since $\Gamma_{\text{sh}} - 1 \sim 0.04(\gamma'_{e, \text{m}}/5)(\epsilon_e/0.2)^{-1}[3(p-2)/(p-1)]^{-1}$, where Γ_{sh} is the Lorentz factor representing the strength of the shock ($\Gamma_{\text{sh}} \sim 1$ for Newtonian shocks). So the acceleration of the protons to ultra-high energy is less efficient than the standard internal shocks. This is particularly the case if the acceleration is mainly via second-order Fermi process, in which the acceleration of particles depends on the shock velocity sensitively.

Even in the standard internal shock model, the generation of 10^{20} eV protons and the production of PeV-EeV neutrinos may be not as promising as that claimed in most literature adopting a proton spectrum $dN/dE \propto E^{-2}$. Such a flat spectrum is predicted for *Newtonian* shocks and has been confirmed by the supernova remnant observations. But the typical MeV spectrum $F_\nu \propto \nu^{-1.25}$ (Preece et al. 2000) of GRBs suggests $dN/dE \propto E^{-2.5}$, supposing the accelerated protons and electrons have the same spectrum. The non-detection of > 100 MeV photon emission from most

GRBs implies soft electron (possibly) and proton spectra. Given a proton spectrum $dN/dE \propto E^{-2.22}$ that is predicted in the relativistic shock acceleration model (the First-order Fermi mechanism), the kinetic energy of the ejecta needs to be ~ 100 times of the γ -ray radiation energy if GRBs are indeed the main source of the observed $\sim 10^{20}$ eV cosmic rays (see Dermer 2008, and the reference therein). In other words, the GRB efficiency should be as low as $\sim 1\%$. If correct, the number of protons at $E \sim 10^{16}$ eV will be quite a few times what assumed in Guetta et al. (2004). Correspondingly the PeV neutrino flux will be higher. However, the current afterglow modeling usually yields a typical GRB efficiency $\sim 10\%$ (e.g., Fan & Piran 2006; Zhang et al. 2007) or larger (e.g., Panaitescu & Kumar 2002; Granot et al. 2006). Below we discuss a new possibility—The proton spectrum is curved. In the “low-energy” part, the spectrum may be steepened significantly by the leakage of the very high energy cosmic rays from the ejecta (see Hillas et al. 2005, and the references therein). The “high-energy” spectrum part may be a lot flatter. For example, in the numerical simulation of cosmic rays accelerated in some supernova remnants, a spectrum $dN/dE \propto E^{-1.7}$ at the high energy part is obtained (e.g., Volk et al. 2002; Berezhko et al. 2003). If holding for GRBs as well and GRBs are the main source of the 10^{20} eV cosmic rays, the PeV neutrino spectrum will be harder than that predicted in Guetta et al. (2004). For instance, the neutron spectra $\epsilon_\nu^2 dN/d\epsilon_\nu \propto \epsilon_\nu^0$ and $\epsilon_\nu^2 dN/d\epsilon_\nu \propto \epsilon_\nu^{-2}$ in their Fig.3 will be hardened by a factor of $\epsilon_\nu^{0.3}$. But the total flux may be just $\sim 10\%$ times that predicted in Guetta et al. (2004) because in this scenario the protons are not as many as that suggested in a flat spectrum $dN/dE \propto E^{-2}$ for $E \ll 10^{20}$ eV.

There is a process, ignored in some previous works, that can enhance the detection prospect a little bit. After the pions (muons) are generated, the high energy pions (muons) will lose energy via synchrotron radiation before decaying, thus reducing the energy of the decay neutrinos (e.g. Guetta et al. 2004). As a result, above $\epsilon_{\nu\mu}^c \sim \frac{10^{17}}{1+z} \epsilon_e^{1/2} \epsilon_B^{-1/2} L_{\gamma, 52}^{-1/2} \Gamma_{i, 2.5}^4 \delta t_{v, -2}$ eV ($\epsilon_{\nu\mu, \nu e}^c \sim \epsilon_{\nu\mu}^c / 10$), the slope of the corresponding neutrino spectrum steepens by 2, where L_γ is the luminosity of the γ -ray emission (Guetta et al. 2004). However we do not suggest a smooth spectral transition around $\epsilon_{\nu\mu}^c$ or $\epsilon_{\nu\mu, \nu e}^c$ because the cooling of pions (muons) will cause a pile of particles at these energies (see also Murase & Nagataki 2006). A simple estimate suggests that the number of neutrinos in the energy range $(0.5, 1)\epsilon_{\nu\mu}^c$ should be enhanced by a factor of ~ 3 . A schematic plot of the muon neutrino spectrum in the standard internal shock model is shown in Fig.7.

5 CONCLUSION

In the pre-Fermi era, it is widely expected that significant GeV emission will be detected in a good fraction of bright GRBs if they are powered by un-magnetized internal shocks (e.g., Pilla & Loeb 1998; Pe’er & Waxman 2004; Gupta & Zhang 2007; Fan & Piran 2008). The detection of a distinct excess at GeV-TeV energies, the SSC radiation component of such shocks, will be a crucial evidence for the standard fireball model. The non-detection of the GeV spectrum excess in almost all Fermi bursts (Abdo et al. 2009) is a surprise but does not impose a tight constraint on the models. For example, in the standard internal shock model, the non-detection can be attributed to a too large $h\nu_{\text{m, SSC}} \sim \text{TeV}$ and a relative low $h\nu_{\text{cut}} \sim \text{GeV}$. Some alternatives, such as the photosphere-internal shock model, the magnetized internal shock model and the photosphere-gradual magnetic dissipation model, can be in agree-

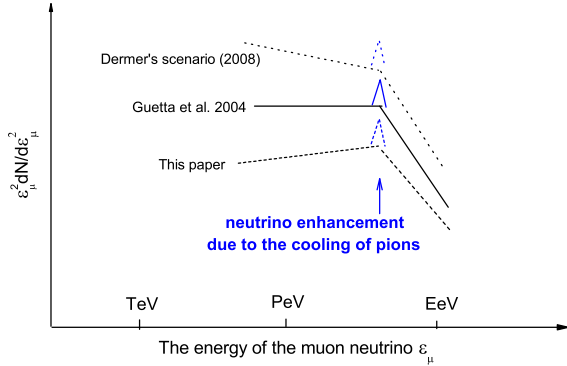


Figure 7. The schematic plot of the PeV muon neutrino spectrum in the standard internal shock model.

Table 2. The physical reasons for the lack of GeV spectrum excess in most GRBs.

model	the physical reason
standard internal shocks	$h(\nu_{m,ssc}, \nu_{cut}) \sim (\text{TeV}, \text{GeV})$
photosphere-internal shocks	very small $\gamma'_{e,m}$ and $\gamma'_{e,c}$
magnetized internal shocks	soft synchrotron spectrum and weak SSC
photosphere-gradual magnetic dissipation	very small $\gamma'_{e,m}$ and $\gamma'_{e,c}$

ment with the data, too (see Tab.2 for a summary). We attribute the delay in the onset of LAT detection in quite a few Fermi bursts to the unfavorable condition for GeV emission of the early outflow (see section 2.2 for details).

With the polarimetry of GRBs people can potentially distinguish between some prompt emission models (see Tab.1 for a summary; see also Toma et al. 2009). We show in section 3.1 that in the photosphere-internal shock model the linear polarization degree is roughly anti-correlated with the weight of the thermal component and will be highly frequency-dependent. Such a unique behavior, if detected, labels its physical origin. However, a moderate/high linear polarization level is expected only when the line of sight is outside of the cone of the ejecta (i.e., $\theta_v > \theta_j$). In addition, $\theta_v - \theta_j \lesssim 1/\Gamma_i$ is needed otherwise the burst will be too weak to perform the gamma-ray polarimetry. Consequently the detection prospect is not very promising.

In this work we have also briefly discussed the detection prospect of prompt PeV neutrinos from GRBs. The roles of the intrinsic spectrum of the protons and the cooling of pions (muons) have been outlined. The latter always increases the neutrino numbers at the energies $\epsilon_{\nu\mu}^c$ or $\epsilon_{\nu\mu, \nu e}^c$ by a factor of 3. The former, however, is uncertain. If the protons have an intrinsic spectrum $dN/dE \propto E^{-2.22}$ and have a total energy about tens times that emitted in gamma-rays, the detection prospect would be as good as, or even better than that presented in Guetta et al. (2004). If the proton spectrum traces that of the electrons, i.e., typically $dN/dE \propto E^{-2.5}$, the detection prospect would be discouraging.

ACKNOWLEDGMENTS

We thank the anonymous referee for very helpful suggestions/comments and Drs. X. F. Wu, K. Toma, and Y. C. Zou for communication. This work was supported in part by the Danish National Science Foundation, Chinese Academy of Sciences, National basic research program of China (grant 2009CB824800), and the National Natural Science Foundation of China (grant 10673034).

REFERENCES

- Abdo A. A., et al., 2009, *Science*, 323, 1688
 Aharonian F. A., Atoyan A. M., 1981, *Ap&SS*, 79, 321
 Band D. et al., 1993, *ApJ*, 413, 281
 Berezhko E. G., Pühlhofer G., Vöolk H. J., 2003, *A&A*, 400, 971
 Berestetskii V. B., Lifshitz E. M., Pitaevski L. P., 1982, *Quantum Electrodynamics*, Oxford OX3 OBW, England
 Boggs S. E., et al., 2006, *New A. Rev.*, 50, 604
 Bosnjak Z., Daigne F., Dubus G., 2009, *A&A* (arXiv:0811.2956)
 Bouvier A., 2008, *GCN Circ.* 8183
 Cheng K. S., Wei D. M., 1996, *MNRAS*, 283, L133
 Coburn W., Boggs S. E., 2003, *Nature*, 423, 415
 Covino S. et al., 1999, *A&A*, 348, L1
 Cutini S., Vasileiou V., Chiang J., 2009, *GCN Circ.* 9077
 Daigne F., Mochkovitch R., 1998, *MNRAS*, 296, 275
 Dermer C. D. 2008, arXiv:0711.2804
 Drenkhahn G., 2002, *A&A*, 387, 714
 Drenkhahn G., Spruit H. C., 2002, *A&A*, 391, 1141
 Duncan R. C., Thompson C., 1992, *ApJ*, 392, L9
 Fan Y. Z., Dai Z. G., Huang Y. F., Lu T., 2002, *ChJAA*, 2, 449
 Fan Y. Z., Piran T., 2006, *MNRAS*, 369, 197
 Fan Y. Z., Piran T., 2008, *Front. Phys. Chin.*, 3, 306
 Fan Y. Z., Wei D. M., 2005, *MNRAS*, 364, L42
 Fan Y. Z., Wei D. M., Wang C. F., 2004a, *A&A*, 424, 477
 Fan Y. Z., Wei D. M., Zhang B. 2004b, *MNRAS*, 354, 1031
 Fan Y. Z., Xu D., Wei D. M., 2008, *MNRAS*, 387, 92
 Fan Y. Z., Zhang B., Proga D., 2005, *ApJ*, 635, L129
 Fenimore E. E., in 't Zand J. J. M., Norris J. P., Bonnell J. T., Nemiroff R. J. 1995, *ApJ*, 448, L101
 Fishman G. J., Meegan C. A., 1995, *ARA&A*, 33, 415
 Ghisellini G., Celotti A. 1999, *ApJ*, 511, L93
 Giannios D., 2007, *A&A*, 480, 305
 Giannios D., Spruit H. C., 2005, *A&A*, 430, 1
 Gotz D., Laurent P., Lebrun F., Daigne F., Bosnjak Z., 2009, *ApJ*, 695, L208
 Granot J., 2003, *ApJ*, 596, L17
 Granot J., Königl A., Piran T. 2006, *MNRAS*, 370, 1946
 Greiner J., et al., 2009, *A&A*, submitted (arXiv:0902.0761)
 Gruzinov A., 1999, 525, L29
 González M. M., Dingus B. L., Kaneko Y., Preece R. D., Dermer C. D., Briggs M. S., 2003, *Nature*, 424, 749
 Guetta, D., Hooper, D., Aliarez-Muniz, J., Halzen, F., Reuveni, E. 2004, *Astropart. Phys.*, 20, 429
 Gupta N., Zhang B., 2007, *MNRAS*, 380, 78
 Hillas A. M., 2005, *J. Phys. G: Nucl. Part. Phys.*, 31, R95
 Hill J. E., et al., 2008, *AIPC*, 1065, 331
 Hurley K., Dingus B. L., Mukherjee R., et al., 1994, *Nature*, 372, 652
 Ioka K., Murase K., Toma K., Nagataki S., Nakamura T., 2007, *ApJ*, 670, L77
 Jin Z. P., Fan Y. Z., 2007, *MNRAS*, 378, 1043

- Katz J. I., Piran T., Sari R. 1998, *Phys. Rev. Lett.*, 80, 1580
 Keshet U., 2006, *Phys. Rev. Lett.* 97, 221104
 Keshet U., Waxman E., 2005, *Phys. Rev. Lett.*, 94, 111102
 Klebesadel R. W., Strong I. B., and Olson R. A., 1973, *ApJ*, 182, L85
 Kobayashi S., Piran T., Sari R., 1997, *ApJ*, 490, 92
 Kumar P., 1999, *ApJ*, 523, L113
 Kumar P., Panaitescu A., 2003, *MNRAS*, 346, 905
 Lithwick Y., Sari R., 2001. *ApJ*, 555, 540
 Lyutikov M., Blandford R., 2003 (arXiv:astro-ph/0312347)
 Lyutikov M., Pariev V. I., Blandford R. D. 2003, *ApJ*, 597, 998
 MacFadyen A. I., Woosley S. E. 1999, *ApJ*, 524, 262
 McGlynn S. et al., 2007, *A&A*, 466, 895
 McGlynn S. et al., 2009, *A&A*, in press (arXiv:0903.5218)
 Mészáros P., 2002, *ARA&A*, 40, 137
 Mészáros P., Rees M. J., 2000, *ApJ*, 530, 292
 Morlino G., Blasi P., Vietri M., 2007a, *ApJ*, 658, 1069
 Morlino G., Blasi P., Vietri M., 2007b, *ApJ*, 662, 980
 Mundell C. G., et al., 2007, *Science*, 315, 1822
 Murase K., Nagataki S., 2006, *Phys. Rev. D.*, 73, 063002
 Nakar E., Piran T., Waxman E., 2003, *JCAP*, 0310, 005
 Narayan R., Paczyński B., Piran T., 1992, *ApJ*, 395, L83
 Norris J. P., Nemiroff R. J., Bonnell J. T., Scargle J. D., Kouveliotou C., Paciesas W. S., Meegan C. A., Fishman G. J. 1996, *ApJ*, 459, 393
 Nousek, J. A., et al., 2006, *ApJ*, 642, 389
 Ohno M., McEnery J., Pelassa V., 2009a, *GCN Circ.* 8903
 Ohno M., Cutini S., McEnery J., Chiang J., Koerding E., 2009b, *GCN Circ.* 9021
 Omodei N., 2008, *GCN Circ.* 8407
 Paczyński B., Xu G. H., 1994, *ApJ*, 427, 708
 Panaitescu A., Kumar P., 2002, *ApJ*, 571, 779
 Pe'er A., 2008, *ApJ*, 682, 463
 Pe'er A., Mészáros P., Rees M. J. 2005, *ApJ*, 635, 476
 Pe'er A., Mészáros P., Rees M. J. 2006, *ApJ*, 642, 995
 Pe'er A., Waxman E., 2004, *ApJ*, 613, 448
 Pilla R. P., Loeb A., 1998, *ApJ*, 494, L167
 Piran T., 1999, *Phys. Rep.*, 314, 575
 Piran T., Sari R., Zou Y. C., 2009, *MNRAS*, 393, 1107
 Preece R. D., Briggs M. S., Mallozzi, R. S., Pendleton G. N., Paciesas W. S., Band D. L. 2000, *ApJS*, 126, 19
 Rees M. J., Mészáros P., 1994, *ApJ*, 430, L93
 Rees M. J., Mészáros P., 2005, *ApJ*, 628, 847
 Rutledge R. E., Fox D. B., 2004, *MNRAS*, 350, 1288
 Ryde F., 2005, *ApJ*, 625, L95
 Ryde F., Björnsson C., Kaneko Y., Mészáros P., Preece R., Batelino M., 2006, *ApJ*, 652, 1400
 Ryde F., Pe'er A., 2009, *ApJ* submitted (arXiv:0811.4135)
 Sari R., Esin A. A., 2001, *ApJ*, 548, 787
 Sari R., Piran T., Narayan R., 1998, *ApJ*, 497, L17
 Sironi L., Spitkovsky, A., 2009, *ApJ*, submitted (arXiv:0901.2578)
 Spruit H. C., Daigne F., Drenkhahn G., 2001, *A&A*, 369, 694
 Thompson C., 1994, *MNRAS*, 270, 480
 Thompson C., Mészáros P., Rees M. J., 2007, *ApJ*, 666, 1012
 Toma K., et al., 2009, *ApJ* in press (arXiv:0812.2483)
 Usov V. V., 1992, *Nature*, 270, 480
 Usov V. V., 1994, *MNRAS*, 267, 1035
 van Paradijs J, Kouveliotou C., Wijers R. A. M. J., 2000, *ARA&A*, 38, 379
 Vietri M., 1995, *ApJ*, 453, 883
 Völk H. J. et al., 2002, *A&A*, 396, 649
 Waxman E., 1995, *Phys. Rev. Lett.*, 75, 386
 Waxman E., 2003, *Nature*, 423, 388
 Waxman E., Bahcall J. N., 1997, *Phys. Rev. Lett.*, 78, 2292
 Wijers R. A. M. J., et al., 1999, *ApJ*, 523, L33
 Willis D. R. et al., 2005, *A&A*, 439, 245
 Zhang B., et al. 2006, *ApJ*, 642, 354
 Zhang B., et al., 2007, *ApJ*, 655, 989
 Zhang B., Kobayashi S., Mészáros P. 2003, *ApJ*, 595, 950
 Zhang B., Mészáros P., 2002, *ApJ*, 581, 1236
 Zhang B., Mészáros P. 2004, *Int. J. Mod. Phys. A*, 19, 2385
 Zhang W. Q., Woosley S. E., MacFadyen A. I., 2004, *ApJ*, 586, 356
 Zou Y. C., Fan Y. Z., Piran T., 2009, *MNRAS*, in press (arXiv:0811.2997)